

# Long-range Forecasting as a Past Value Problem: Using Scaling to Untangle Correlations and Causality

L. Del Rio Amador<sup>1</sup>, S. Lovejoy<sup>1</sup>

<sup>1</sup>Physics, McGill University, 3600 University St., Montreal, Que. H3A 2T8, Canada.

Corresponding author: Lenin Del Rio Amador ([delrio@physics.mcgill.ca](mailto:delrio@physics.mcgill.ca))

## Key Points:

- Scaling-based long-range stochastic forecasting is a past value problem not an initial value problem.
- Granger causality shows that while spatial correlations exist in the temperature field, they cannot be used to improve on predictions based on historical data of individual infinite time series.
- The statistics and teleconnection patterns of the real-world can be reproduced with stochastic simulations with a total lack of causal relationships.

## Abstract

Conventional long-range weather prediction is an initial value problem that uses the current state of the atmosphere to produce ensemble forecasts. Purely stochastic predictions for long-memory processes are “past value” problems that use historical data to provide conditional forecasts. Teleconnection patterns, defined from cross-correlations, are important for identifying possible dynamical interactions, but they do not necessarily imply causation. Using the precise notion of Granger causality, we show that for long-range stochastic temperature forecasts, the cross-correlations are only relevant at the level of the innovations – not temperatures. This justifies the Stochastic Seasonal to Interannual Prediction System (StocSIPS) that is based on a (long memory) fractional Gaussian noise model. Extended here to the multivariate case, (m-StocSIPS) produces realistic space-time temperature simulations. Although it has no Granger causality, emergent properties include realistic teleconnection networks and El Niño events and indices.

## 1 Introduction

For forecasts over the weather regime – below the  $\approx 10$  day deterministic predictability limit – Numerical Weather Prediction (NWP) and General Circulation Models, (GCMs) have been highly successful, yet for longer term macroweather (“long range”) forecasts, their skill is disappointing. This has motivated the development of stochastic alternatives. Successful stochastic forecasts require causal models and the search for causality typically starts with correlations. In the last years, two stochastic strands have emerged each inspired by different sources of strong correlations. A particularly well studied constellation of correlations are associated with large scale spatial structures – teleconnections – as vividly displayed in climate networks [e.g.: (Donges et al., 2009b; Ludescher et al., 2014)]. Teleconnection-inspired forecast models often use climate (especially El Niño) indices [see (Brown & Caldeira, 2020; Eden et al., 2015)]. An alternative source of correlations upon which to base causal models is the system’s long range memory (Blender & Fraedrich, 2003; Bunde et al., 2005; Rypdal et al., 2013; Varotsos et al., 2013), a consequence of temporal scaling, itself associated with long range

40 spatial scaling, a basic property of the governing equations that is well respected by both GCMs  
41 and the empirical data [(Palmer, 2019), see also the review (Lovejoy & Schertzer, 2013)].

42 At the moment, these strands are at virtual antipodes. Models based on teleconnections  
43 use only data from a few months – they are Markovian, short (exponential) memory models that  
44 get their skill largely from spatial information. In this, they are almost as extreme as GCMs that  
45 are zero-memory, initial value models based purely on the spatial information at  $t = 0$ . In  
46 contrast, the scaling, long memory Stochastic Seasonal to Interannual Prediction System  
47 (StocSIPS) model is at the opposite extreme (Del Rio Amador & Lovejoy, 2019, 2020). For each  
48 pixel, it uses historical past data to forecast the future - but uses no other data as co-predictors: it  
49 is a purely “past value” model. In spite of this apparent deficiency, for monthly, seasonal, and  
50 annual temperature forecasts StocSIPS’ skill already rivals – or exceeds – those of GCMs.

51 This paper attempts to answer the obvious question: is it possible to make a model that  
52 combines strong spatial correlations and long memory to produce even more skillful forecasts?  
53 While it is well known that correlations and causality are not synonymous, the precise  
54 relationship between the two is often unclear and there are no general tools for untangling them.  
55 However, the present case is an important exception: the problem of improving StocSIPS using  
56 spatial co-predictors can be precisely answered by using the theoretical framework of Granger  
57 causality (Granger, 1969).

58 Two series are Granger causally related iff one can be used as a skillful co-predictor of  
59 the other. Therefore, it suffices to enquire as to the Granger causality of the space-time StocSIPS  
60 model. If the temperature teleconnections have no Granger causality, then they will not improve  
61 StocSIPS forecasts. In the first part of the paper we propose a multivariate surface temperature  
62 model (m-StocSIPS) for which the uncoupled regional StocSIPS model gives the optimal  
63 forecast. m-StocSIPS also reproduces the empirical cross-correlation structure over a wide range  
64 of time lags. This is made more convincing by making simulations that display numerous  
65 realistic but emergent model properties including spatial teleconnection networks, realistic El  
66 Niño patterns and indices. The optimal m-StocSIPS predictor at a given location is obtained from  
67 its own past if the series is long enough. Even strongly spatially correlated series from other  
68 locations do not help improve the skill, teleconnection correlations may be seductive, but without  
69 Granger causality, they are misleading.

## 70 **2 Methods**

### 71 **2.1 Stochastic modeling of the temperature anomalies**

72 In macroweather temperature anomalies at position  $\mathbf{x}$  (after removing the annual cycle)  
73 can be modeled as a trend-stationary process:

$$74 \quad T_{\text{anom}}(\mathbf{x}, t) = T_{\text{anth}}(\mathbf{x}, t) + T(\mathbf{x}, t), \quad (1)$$

75 where  $T(\mathbf{x}, t)$  is a stochastic stationary component and  $T_{\text{anth}}(\mathbf{x}, t)$  is a deterministic low-  
76 frequency response to anthropogenic forcings as in (Del Rio Amador & Lovejoy, 2019).

77 The stationary stochastic  $T(\mathbf{x}, t)$ , is the zero-mean residual natural variability that  
78 includes “internal” variability and the response of the system to other natural forcings (e.g.:  
79 volcanic and solar). These anomalies can be predicted by modelling each position independently  
80 using an univariate representation [the regional StocSIPS model presented in (Del Rio Amador

81 & Lovejoy, 2020), hereafter DRAL]. However, to investigate whether forecasts for individual  
 82 series can be improved using other data, a multivariate framework is needed. A quasi-Gaussian  
 83 process, stationary in time, but inhomogeneous in space has a multivariate continuous-in-time  
 84 Wold representation (moving average of infinite order MA( $\infty$ )) (Box et al., 2008; Brockwell &  
 85 Davis, 1991; Wold, 1938):

$$86 \quad T_i(t) = \sum_j \int_{-\infty}^t \kappa_{ij}(t-t') \gamma_j(t') dt'. \quad (2)$$

87 The index “ $i$ ” is a subscript indicating the spatially discrete position (“pixel”), the matrix  $\kappa_{ij}(t)$   
 88 is a kernel specifying the MA process and the innovations,  $\gamma_i(t)$ , are normalized Gaussian white  
 89 noise processes with  $\langle \gamma_i(t) \rangle = 0$ ,  $\langle \gamma_i^2(t) \rangle = 1$  and cross-correlation matrix:

$$90 \quad \rho_{ij}(t-t') = \langle \gamma_i(t) \gamma_j(t') \rangle = a_{ij} \delta(t-t'), \quad (3)$$

91 where  $\delta(t)$  is the Dirac function,  $\langle \cdot \rangle$  denotes ensemble averaging and  $-1 < a_{ij} < 1$ . This “delta-  
 92 correlated” innovation temporal structure implies that the latter are totally unpredictable and is  
 93 the key property below.

94 The cross-covariance for time lag  $\Delta t > 0$  for the temperature is:

$$95 \quad C_{ij}(\Delta t) = \langle T_i(t) T_j(t + \Delta t) \rangle = \sum_m \sum_n \int_0^{\infty} \kappa_{im}(t') \kappa_{jn}(t' + \Delta t) a_{mn} dt', \quad (4)$$

96 hence the cross-correlation is:

$$97 \quad R_{ij}(\Delta t) = \frac{C_{ij}(\Delta t)}{\sqrt{C_{ii}(0) C_{jj}(0)}}. \quad (5)$$

98 Since the process is Gaussian with zero mean, it is completely determined by the  
 99 correlation structure. In the macroweather regime – with the possible exception of extremes –  
 100  $T_i(t)$  is nearly Gaussian in time, but multifractal in space and the statistics of its fluctuations are  
 101 scale-invariant over wide ranges (Lovejoy, 2018; Lovejoy et al., 2018; Lovejoy & Schertzer,  
 102 2013). The scaling behaviour in time implies that there are power-law correlations and hence  
 103 potentially a large memory that can be exploited. The simplest relevant scaling process is the  
 104 statistically stationary fractional Gaussian noise (fGn) process.

105 The fGn based StocSIPS model was first developed for monthly and seasonal forecast of  
 106 globally averaged temperature (Lovejoy et al., 2015; Del Rio Amador & Lovejoy, 2019).  
 107 Recently, DRAL extended StocSIPS to the regional prediction of  $T_i(t)$ , where each grid point  
 108 was considered as an independent time series. This univariate representation using a resolution  $\tau$   
 109 fGn process (see the supporting information) can be extended to the multivariate case with the  
 110 kernel:

$$111 \quad \kappa_{ij}(t) = \delta_{ij} \frac{1}{\tau} \frac{c_{H_i} \sigma_{T_i}}{\Gamma[H_i + 3/2]} \left[ t^{H_i+1/2} - (t-\tau)^{H_i+1/2} \theta(t-\tau) \right], \quad (6)$$

112 where  $\theta(t)$  is the Heaviside (step) function,  $\Gamma$  is the Gamma function,  $H_i \in (-1,0)$  is the  
 113 fluctuation exponent characterizing the scaling of the fluctuations in time,  $\sigma_{T_i}$  is the standard

114 deviation,  $c_{H_i}$  is a normalization constant and  $\delta_{ij}$  is the Kronecker  $\delta$ . The different temperature  
 115 series,  $T_i(t)$ , are correlated, and the spatial correlation structure is inherited from the innovation  
 116 cross-correlations,  $a_{ij}$ . The presence of the Kronecker  $\delta$  in Eq. (6) implies that the temperature at  
 117 grid point “ $i$ ” is an fGn with parameters  $H_i$  and  $\sigma_{T_i}$ .

118 In DRAL it was shown that the fGn model (Eq. (6)) is an accurate univariate  
 119 representation of the natural temperature variability for most of the globe. However, in the  
 120 tropical ocean, the fGn model approximates the temperature increments, meaning that the actual  
 121 temperature variability is modelled as a fractional Brownian motion (fBm) process with  
 122 fluctuation exponent  $H_i \in (0,1)$  (see Fig. 1(a)), although cut-off at multi-annual scales. The  
 123 fluctuation exponents of fBm and fGn are related as  $H_{\text{fBm}} = H_{\text{fGn}} + 1$ . Both cases are high-  
 124 frequency approximations of the more general fractional relaxation noise (fRn) process,  
 125 introduced in (Lovejoy, 2019; Lovejoy et al., 2020).

126 The use of a parametric model considerably reduces the number of parameters and  
 127 clarifies their interpretation. m-StocSIPS is fully determined by the symmetric innovation cross-  
 128 covariance matrix  $a_{ij}$ , the amplitudes of the temperature fluctuations  $\sigma_{T_i}$ , and the memory  
 129 exponents  $H_i$ . These characterize the internal dynamics; for example low values of  $\sigma_{T_i}$  over the  
 130 oceans are a consequence of the greater heat capacity and thermal inertia and  $H_i$  characterizes the  
 131 memory associated with the multiscale energy storage mechanisms (Lovejoy, 2020; Lovejoy et  
 132 al., 2020).

133 m-StocSIPS is defined by  $N(N + 3)/2$  parameters; in comparison, a vector  
 134 autoregressive order  $p$  model (VAR( $p$ )) needs  $pN^2$  values (Box et al., 2008; Brockwell & Davis,  
 135 1991) and for long-memory processes,  $p$  is large. These “black box” type models suffer from  
 136 opaque physical interpretations, and their large number of VAR parameters makes them unstable  
 137 and subject to overfitting. The same is true for general vector autoregressive-moving average  
 138 VARMA( $p, q$ ) models.

139 Ultimately, the adequacy of a model must be checked. In this case, the diagnostics are  
 140 primarily based on the examination of the whiteness and time-independence of the residual  
 141 vectors  $\gamma_i(t)$ , which are obtained by inverting Eq. (2) with the estimated parameters. The  
 142 whiteness was verified in DRAL using the theory in Appendix 1 of (Del Rio Amador & Lovejoy,  
 143 2019). To verify the time-independence of the innovations (Eq. (3)), there exist many “goodness-  
 144 of-fit” tests based on the residual cross-covariance matrices at several lags (Ali, 1989; Hosking,  
 145 1980; Li & McLeod, 1981; Poskitt & Tremayne, 1982). In our case, they are either impractical –  
 146 the matrices have more than  $1.1 \cdot 10^8$  elements – or impossible since there is only one realization  
 147 of our planet. Nevertheless, a visual inspection of the residual cross-correlation matrices for  
 148 different lags (shown in Fig. S2 in the supporting information) may be enough. Our results  
 149 indicate that m-StocSIPS is a good approximation, confirmed in Sect. 3.3 using global  
 150 simulations that convincingly reproduce the space-time patterns (Fig. 2). Aside from minor  
 151 numerical approximations, StocSIPS predictions presented in DRAL are optimal m-StocSIPS  
 152 predictions in the minimum mean square error framework, explaining the high StocSIPS forecast  
 153 skill.

### 154 **2.3 Correlation, causality and Granger causality**

155 m-StocSIPS uses an fGn model for most of the globe (where  $H_i < 0$ ) and a (truncated)  
 156 fBm model for the tropical ocean (where  $H_i > 0$ ). The cross-correlation structure for the

157 temperature anomalies is thus determined by three kinds of interaction: 1) fGn-fGn, 2) fGn-fBm  
 158 and 3) fBm-fBm. The fGn-fGn cross-correlation can be obtained directly by using Eq. (6) in Eq.  
 159 (4). The exact result is given in the supporting information (Eq. S22). Similar expressions can be  
 160 obtained for the other two cases (Coeurjolly et al., 2010).

161 While fGn is a stationary process and fGn-fGn cross-correlations only depend on the lag  
 162  $\Delta t$ , this is not the case for fBm. Nevertheless, under some approximations for long enough finite  
 163 time series, it is possible to obtain expressions that only depend on  $\Delta t$  [see (Delignières, 2015)].  
 164 The cross-correlations for  $\Delta t \gg \tau$  ( $\tau$  is the temporal resolution of the time series, i.e. 1 month)  
 165 are:

166 Case 1: fGn-fGn ( $H_i < 0$  and  $H_j < 0$ ),

$$167 R_{ij}(\Delta t) \sim \varphi_{H_i, H_j} a_{ij} (\Delta t / \tau)^{H_i + H_j} . \quad (7)$$

168 Cases 2 and 3: fGn-fBm and fBm-fBm ( $H_i > 0$  or/and  $H_j > 0$ ),

$$169 R_{ij}(\Delta t) \sim \phi_{H_i, H_j} a_{ij} \left[ 1 - (\Delta t / \tau_r^{ij})^{H_i + H_j} \right] , \quad (8)$$

170 for  $\Delta t \ll \tau_r^{ij}$ , where  $\tau_r^{ij}$  is a characteristic relaxation time related to the ocean weather-ocean  
 171 macroweather transition (Lovejoy, 2019; Lovejoy et al., 2018; Del Rio Amador & Lovejoy,  
 172 2020), and  $\varphi_{H_i, H_j}$  and  $\phi_{H_i, H_j}$  are proportionality constants that depend on  $H_i$  and  $H_j$  (see Eq. S25  
 173 in the supporting information). As expected, these expressions coincide with the high-frequency  
 174 approximations of the stationary fRn cross-correlations for  $H_i$  and  $H_j$ .

175 Equations (7) and (8) imply that the cross-correlation structure of the temperature field  
 176 has a spatial correlation component given by the matrix  $a_{ij}$ , and a temporal component  
 177 determined by the memory dependence of the individual series ( $H_i$  and  $H_j$ ). In this sense, they  
 178 are similar, but more general than the average Statistical Space-Time Factorization (SSTF)  
 179 proposed earlier by (Lovejoy & de Lima, 2015). For a given location  $i$  and lag  $\Delta t$ , the cross-  
 180 correlation with any other location  $j$  will be higher for series whose past is important (large  $H_i$ )  
 181 as compared to series with short memories (small  $H_i$ ).

182 Now consider the prediction problem for the general process given by Eq. (2). Since the  
 183 process is Gaussian, we use the minimum mean square error framework. Although correlations  
 184 play an important role in the statistical description and in pattern identification, it is wrong to  
 185 infer causality based on the lagged cross-correlation structure alone. In the words of (Buchanan,  
 186 2012): “Not only does correlation not imply causality, but lack of correlation needn’t imply a  
 187 lack of causality either”. A classic example is two correlated systems without any dynamic  
 188 interaction between them but with a common dependence on a third variable. Conversely, there  
 189 are coupled chaotic systems, that exhibit a complete lack of long-term statistical correlation,  
 190 despite sharing a clear cause-effect link (Sugihara et al., 2012).

191 An example from (Barnston, 2014; Lyon & Barnston, 2005) may clarify the discussion.  
 192 They argue that El Niño events *lead* to a cascade of global impacts, e.g.: wet Central Asias.  
 193 However, in GCM terms, a given set of initial conditions is the ultimate cause of both an El Niño  
 194 and a wet season in Central Asia. The chain of events starting from those initial conditions  
 195 explains the mutual correlations without mutual causation. In traditional mechanistic terms, the  
 196 best that can be done to reconcile the two viewpoints is the notion of causal chain (e.g. Bunge,

197 2017). In this fairly qualitative view, the ultimate cause – the initial conditions – triggers a causal  
 198 chain of events in which El Niño is a “proximate” link leading to a wet season in Central Asia.

199 From a stochastic point of view, (Andree, 2019) argues that a time series (e.g. the  
 200 temperature at a given location) has a memory part depending on its own past and a causal part  
 201 from the past at other locations. For short-memory processes, this causal contribution may be  
 202 important, explaining how some empirical models obtain their skill by effectively borrowing  
 203 memory from co-predictors. However, the longer the memory – the more autoregressive steps  
 204 that are needed – the lower the influence of the causal component. In the limit, all the causal  
 205 chain for a given time series may be embedded in its own past, so that GCMs and StocSIPS  
 206 exploit a whole chain of causation, not only the last links in the chain so that their skill is higher  
 207 than models that only exploit proximate causes.

208 The precise tool needed to clarify stochastic causality issues is Granger causality  
 209 (Granger, 1969). We say that the temperature  $T_j$  at location  $j$  fails to Granger-cause the  
 210 temperature  $T_i$ , if for all future times  $t > 0$ , the mean square error (MSE) of a forecast of  $T_i(t)$   
 211 based on its own past ( $T_i(s)$  for  $s \leq 0$ ) is the same as the MSE of a forecast of  $T_i(t)$  based on  
 212 both  $T_i(s)$  and  $T_j(s)$ . The notion of Granger causality is intuitive and provides a much more  
 213 rigorous criterion for causation than simple lagged cross-correlations. While other notions of  
 214 causality exist, Granger causality does imply forecasting ability, which is our only concern here.

215 We now investigate the Granger causality of m-StocSIPS. A necessary and sufficient  
 216 condition for the optimality of an estimator is given by the orthogonality principle (Box et al.,  
 217 2008; Brockwell & Davis, 1991; Palma, 2007; Straškraba, 2007; Wold, 1938), that states that the  
 218 error of the optimal predictor (in a mean square error sense) is orthogonal to any possible  
 219 estimator:

$$220 \quad \langle \hat{T}_i(t) E_i(t) \rangle = 0, \quad (9)$$

221 where  $\hat{T}_i(t)$  is the temperature predictor for position  $i$  at a future time  $t > 0$  and  $E_i(t) = T_i(t) -$   
 222  $\hat{T}_i(t)$  is the error.

223 From the integral representation (Eq. (2)) and given a diagonal kernel  $\kappa_{ij}(t)$  as in Eq. (6),  
 224 we find that the optimal predictor satisfying this principle is:

$$225 \quad \hat{T}_i(t) = \int_{-\infty}^0 \kappa_{ii}(t-t') \gamma_i(t') dt', \quad (10)$$

226 with error:

$$227 \quad E_i(t) = \int_0^t \kappa_{ii}(t-t'') \gamma_i(t'') dt''. \quad (11)$$

228  $E_i$  only depends on future innovations  $\gamma_i(t'')$  ( $t'' > 0$ ), while the estimator,  $\hat{T}_i(t)$ , depends only  
 229 on past innovations  $\gamma_i(t')$  ( $t' < 0$ ). Since the white noise innovations are  $\delta$ -correlated in time  
 230 (Eq. (3)), for any  $i, j$  we have:

$$231 \quad \langle T_j(s) E_i(t) \rangle = 0; \quad s < 0, t > 0. \quad (12)$$

232 This means that any predictor that is a linear combination of past temperature values from  
 233 any position  $j$ , is orthogonal to the error of the predictor obtained from the past at location  $i$ ,  
 234 given by Eq. (10). Hence, the predictor (Eq. (10)) is optimal given the full field  $T(\mathbf{x}, t)$  for  $t \leq 0$ .  
 235 This is a precise statement of Granger causality. Although there are large cross-correlations  
 236 inherited from the innovation matrix  $a_{ij}$  (Eqs. (7) and (8)), the information of past temperatures  
 237 from other locations does not help improve the forecast. For StocSIPS predictions, it is the lack  
 238 of innovation connectivity at non-zero lags that implies that the optimal predictor for any given  
 239 location is obtained from its past. In effect, these occasionally strong spatial correlations “were  
 240 already used” for building the past of any given time series, whose past is therefore enough to  
 241 yield the optimal predictor for that specific series.

## 242 3 Results

### 243 3.1 Empirical cross-correlations

244 Our analysis were based on monthly,  $2.5^\circ$  resolution surface temperatures (T2m:  $73 \times$   
 245  $144 = 10512$  points) from 1948 to 2019 (864 months in total) from the National Centers for  
 246 Environmental Prediction/National Center for Atmospheric Research Reanalysis 1 (Kalnay et al.,  
 247 1996; NCEP/NCAR, 2020).

248 The validity of the univariate fGn (StocSIPS) model was confirmed in DRAL by testing  
 249 the whiteness of the innovations  $\gamma_i(t)$  for every grid point  $i$ , which were obtained by inverting  
 250 the discrete version of Eq. (2) (see the supporting material for the theoretical details). We used  
 251 the fact that a white noise process is a particular case of fGn with fluctuation exponent  $H_\gamma =$   
 252  $-1/2$ . Maximum likelihood estimates for the residuals at 10512 grid points give  $H_\gamma =$   
 253  $-0.498 \pm 0.003$  and standard deviations  $\sigma_\gamma = 1.000 \pm 0.002$ , which confirms that the  
 254 innovations are unit variance  $\delta$ -correlated white noise and hence the adequacy of the fGn model  
 255 for the natural temperature variability in the univariate case.

256 To show that the multivariate model is also realistic, we must check that the lagged cross-  
 257 correlations between the innovations at different locations (Eq. (3)) are negligible. For this  
 258 analysis, we obtained the lagged cross-correlation matrices involving the 10512 grid points for  
 259 the innovations,  $\rho_{ij}(\Delta t)$ , and for the temperature variability,  $R_{ij}(\Delta t)$ , for  $\Delta t$  from 1 to 12  
 260 months. These matrices are shown in the supporting information (Fig. S2) for  $\Delta t = 0, 1, 2$  and 3  
 261 months. For the temperature, the correlations decrease with  $\Delta t$ , but large values are often  
 262 obtained for relatively large lags, following Eqs. (7) and (8). For the innovation cross-  
 263 correlations, the values decrease much faster. For  $\Delta t = 0$ , the elements  $\rho_{ij}(0) = a_{ij}$  are  
 264 relatively large, but even for  $\Delta t = 1$  month, almost all the correlation is lost. This indicates that  
 265 the innovations closely satisfy the discrete version of the time-independence condition Eq. (3).

266 Another way of testing the model is by checking that Eqs. (7) and (8) are good  
 267 approximations of the empirical  $R_{ij}(\Delta t)$ . Fig. 1(a) shows the results for ensembles with similar  
 268  $a_{ij}, H_i$  and  $H_j$  values ( $a_{ij} = 0.5 \pm 0.025$  gives 10490 pairs). Comparisons are shown for the  
 269 three cases (fGn-fGn, fGn-fBm and fBm-fBm):

270 Case 1: fGn-fGn (marked as “+” in Fig.1(a)), we chose the series with  $H_i = -0.1 \pm$   
 271  $0.025$  (red symbol) and  $H_j = -0.3 \pm 0.025$  (yellow), 380 pairs.



272 Case 2: fGn-fBm (marked as “o”), the series with  $H_i = -0.1 \pm 0.025$  (purple) and  $H_j =$   
 273  $0.25 \pm 0.025$  (green), 569 pairs.

274 Case 3: fBm-fBm (marked as “x”), the series with  $H_i = 0.3 \pm 0.025$  (black) and  $H_j =$   
 275  $0.4 \pm 0.025$  (cyan), 323 pairs.

276 Fig. 1(b) shows the average cross-correlations functions of the lag  $\lambda = \Delta t/\tau$  ( $\tau = 1$   
 277 month), with fits from Eqs. (7) and (8). For case 1, we included the dashed red curve  
 278 corresponding to higher order corrections for fRn processes (Lovejoy, 2019; Lovejoy et al.,  
 279 2020). The small values of the cross-correlation innovation pairs (“\*” in the figure) confirm the  
 280 independence of these series. Although the expressions (Eqs. (7) and (8)) are only first order

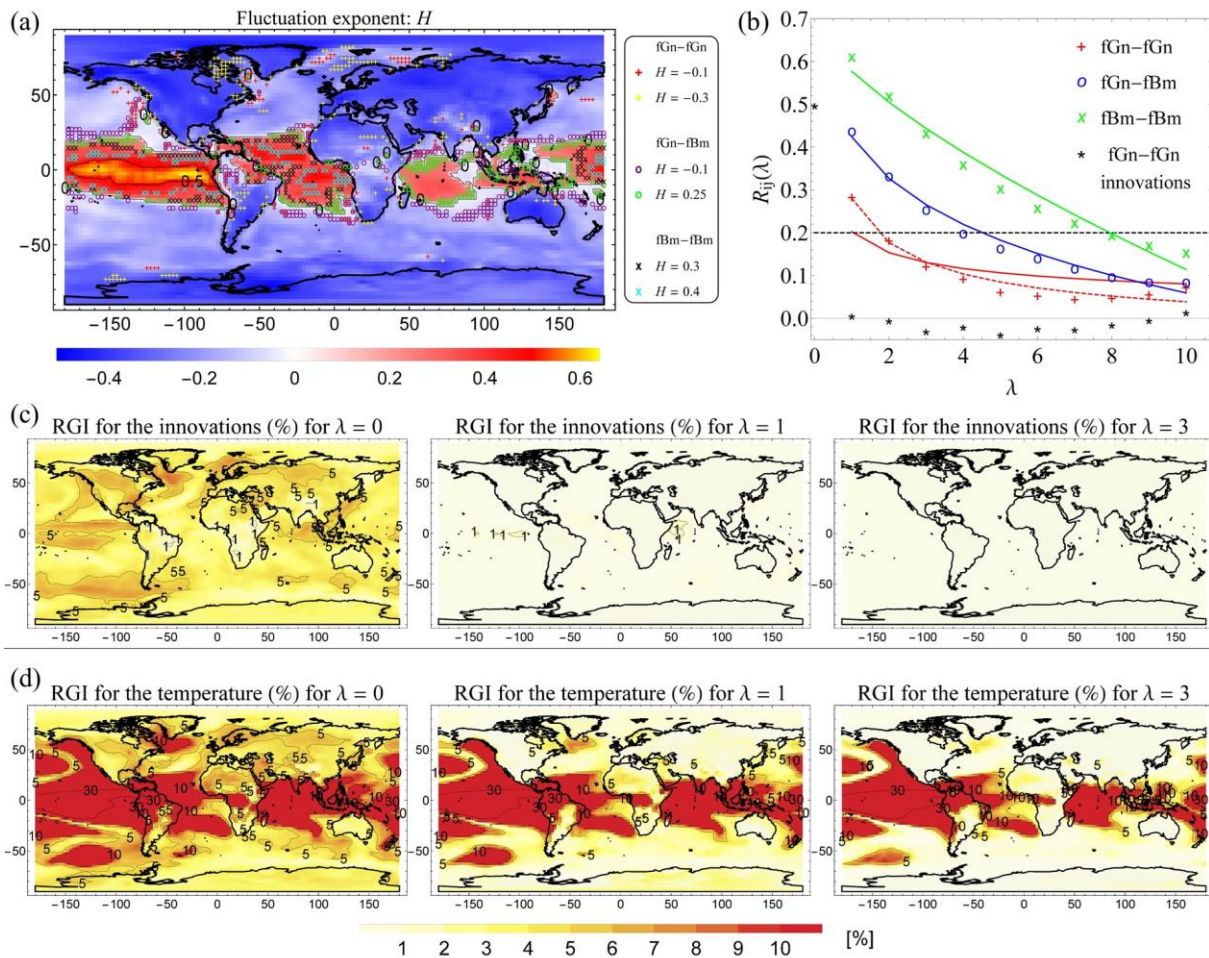


**Fig. 1** (a) Maximum likelihood estimates of the fluctuation exponent,  $H$ . The grid points forming the pairs used to calculate the average ensemble cross-correlations (shown in (b)) are marked as: “+” for fGn-fGn, “o” for fGn-fBm and “x” for fBm-fBm. The colours indicate the values of  $H$ . (b) Average cross-correlations for  $\lambda = 1 - 10$  for the cases 1, 2 and 3 (described in the text), with the corresponding fits from Eqs. (7-8) (we also included in dashed red the curve corresponding to higher order corrections for fRn processes). The average cross-correlations for the pairs of innovations corresponding to the series selected in Case 1 were included as reference (“\*” symbol). (c) Ratio of Global Influence (RGI) for innovations for  $\lambda = 0, 1$  and  $3$ . (d) RGI for temperature anomalies. The RGI for pixel  $i$  was defined as the fraction of the area of the planet for which the cross-correlation  $|R_{ij}(\lambda)| > 0.2$  for all  $j$ .



281 approximations, there is good agreement with the empirical values. This supports the model and  
 282 shows that the correlation structure has an intrinsic spatial component proportional to  $a_{ij}$ , and a  
 283 temporal, memory-dependent component that depends on  $H_i$  and  $H_j$ .

### 284 **3.2 Ratio of global influence**

285 Empirical Orthogonal Functions (EOF) or Principal Component Analysis (PCA)  
 286 decomposition techniques are often used to interpret the lagged cross-correlations (the matrices  
 287  $R_{ij}(\Delta t)$ , Fig. S2). This includes temperature teleconnection patterns, even though – if our model  
 288 is valid – these have no Granger causality. An alternative to EOF teleconnection analysis is  
 289 provided by network analysis (Donges et al., 2009a; Steinhäuser et al., 2012; Tsonis, 2018;  
 290 Tsonis et al., 2006; Yamasaki et al., 2008) based on the zero lag cross-correlations that define the  
 291 area weighted connectivity (AWC).

292 Since the zero-lag statistics have no causal information, we generalized the AWC to  
 293 nonzero lags by defining the ratio of global influence (RGI). The RGI for pixel  $i$  is the fraction of  
 294 the area of the planet for which  $|R_{ij}(\lambda)| > 0.2$ , averaged over all  $j$  (for innovations  $|\rho_{ij}(\lambda)| >$   
 295  $0.2$ ), for zero lags it is equal to the AWC. Values below 0.2 (dashed line in Fig. 1(b)) are  
 296 considered to be of low influence. In climate networks, a threshold of 0.5 is typically used for  
 297 defining connectivity, but innovation correlations – relevant to Granger causality – are much  
 298 weaker, hence 0.2 was chosen

299 Figure 1(c) and (d) shows RGI maps for innovations and temperatures, respectively, for  
 300  $\lambda = 0, 1$  and 3. For the innovations, almost all the correlation is lost for  $\lambda > 0$ , in agreement with  
 301 Eq. (3): there is no significant influence on future values for any pixel. For  $\lambda = 0$ , we see that the  
 302 region of largest innovation influence is the tropical Pacific where  $\text{RGI} \approx 5\%$ . For temperature  
 303 anomalies (panel (d)), much larger correlations and RGIs are obtained. For  $\lambda > 0$ , almost all the  
 304 influence from land disappears, but the ocean's influence is preserved up to around 1 year (not  
 305 shown). Unsurprisingly, the tropical ocean has the largest correlations. As we mentioned earlier,  
 306 this is a consequence of the long memory (large  $H$ , Fig. 1(a)).

307 Rigorously, the orthogonality condition (Eq. (12)) was derived for infinitely long time  
 308 series with complete knowledge of the infinite past. In practice, we only have finite series and for  
 309 each pixel, the memory effects of the unknown past will depend on the  $H$  values. For a fixed,  
 310 finite length of past data, series with  $H$  closer to zero have more past information that can be  
 311 borrowed. In the supporting information, we confirm that there is a small improvement in skill  
 312 using a co-predictor series from different locations, but this improvement decreases with the  
 313 memory,  $m$ , and is very small when sufficient past data points are used to build the predictor (see  
 314 Fig. S3). For 20 months of past data, forecast skill improves by a maximum of 2%, which is  
 315 roughly the noise level of the skill estimates (see Fig. S6). If only a few memory-steps are used,  
 316 then the improvement in skill from borrowing memory from co-predictors is larger, but in all  
 317 cases the combined predictor / co-predictor skill is lower than for the single long-memory  
 318 predictor (see Figs. S4 and S5).

### 319 **3.3 Simulations and emergent properties**

320 At each pixel, m-StocSIPS has the same statistics as StocSIPS, which DRAL showed to  
 321 be quite accurate. However in addition, m-StocSIPS takes into account the spatial correlations: to

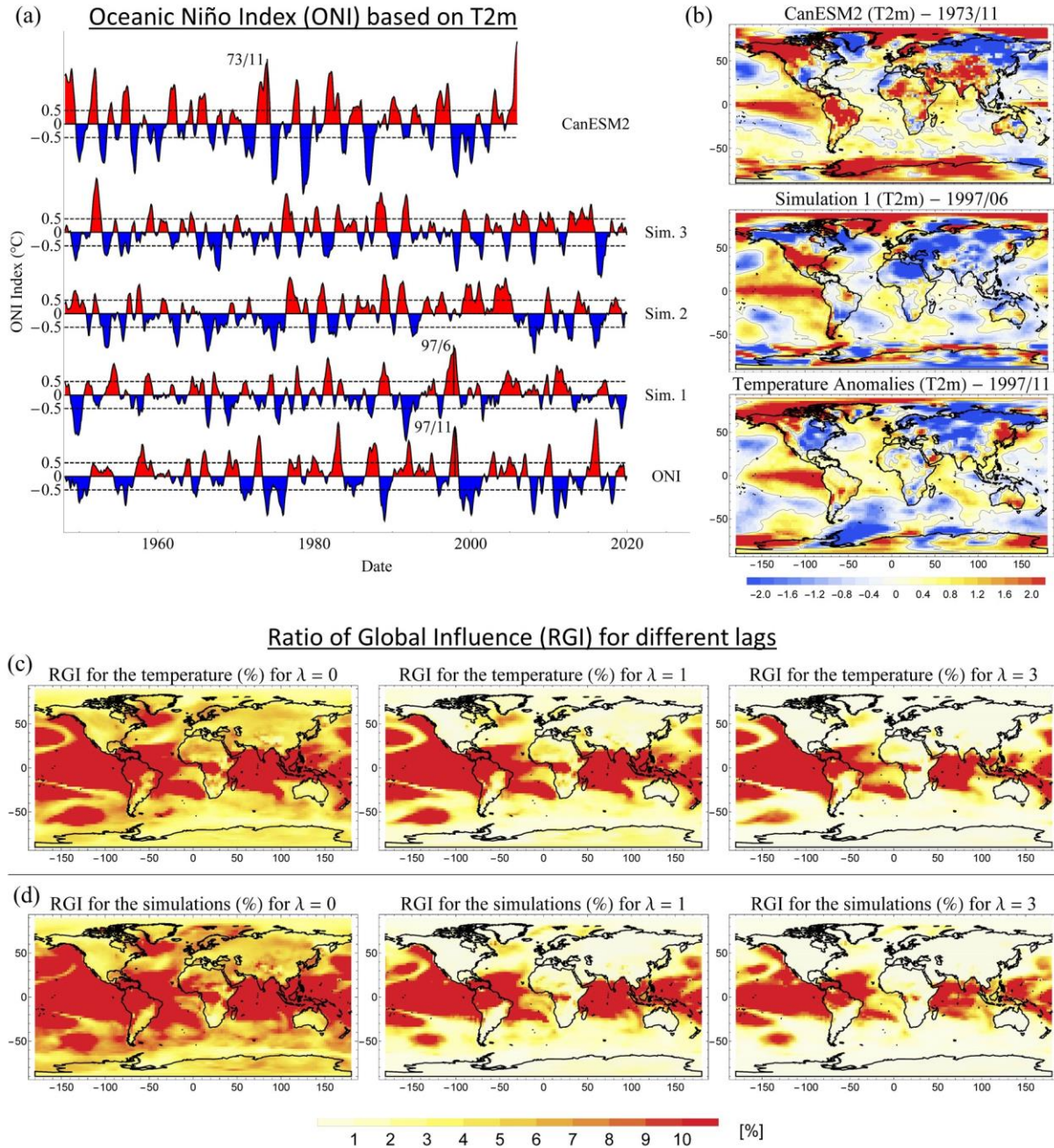


**Fig. 2** (a) Comparison between series of the Oceanic Niño Index (ONI) derived for surface temperature (T2m) as the 3-month running mean of the average over the region (5°N-5°S, 170°W-120°W). In the bottom, we show the series computed from reanalysis (labelled as ONI); in the middle, samples from three different simulations (marked as Sim.1-3) and in the top, the index computed from one of the historical runs of the second generation Canadian Earth System Model (CanESM2) for the period 1948-2005. (b) Canonical anomaly pattern associated with the El Niño peaks marked in the series in Fig. 2(a) for each respective case. (c) Ratio of Global Influence (RGI) for the observational reference dataset for  $\lambda = 0, 1$  and 3. (d) RGI for the Simulation 1 dataset.

322 be a realistic macroweather model it must also reproduce the observed spatial patterns including  
 323 teleconnection networks (AWC, RGI), and El Niño events and indices. Since – just as in GCMs –

324 m-StocSIPS does not put these features in “by hand”, they are emergent model properties that are  
 325 notoriously difficult to reproduce so that their realism (or lack thereof) provide stringent quality  
 326 checks. Using m-StocSIPS simulations, (detailed in Sects. S2 and S7 of the supporting  
 327 information) we now show that indeed, these emergent properties are well reproduced.

328 In order to compare StocSIPS space-time statistical structures to reanalysis and to GCM  
 329 outputs, we produced simulations with the same resolutions and overall length as our reference  
 330 NCEP/NCAR Reanalysis 1 dataset (864 months,  $2.5^\circ$  resolution). Although full movies of the  
 331 model outputs are available (Movie S1), here we focus on El Niño events that are particularly  
 332 difficult to simulate. First consider the Oceanic Niño Index (ONI) derived for surface  
 333 temperature (T2m) as the 3-month running mean of the average over the region ( $5^\circ\text{N}$ - $5^\circ\text{S}$ ,  
 334  $170^\circ\text{W}$ - $120^\circ\text{W}$ ), Fig 2(a). The bottom (“ONI”) is a reanalysis series above which are samples  
 335 from three different m-StocSIPS realizations (“Sim.1-3”, middle). The top series is from a  
 336 historical run of the CanESM2 GCM (CCCma, 2020), the ONI was estimated after standard  
 337 detrending (but without variance adjustments).

338 Except for the larger GCM amplitude, the time series in Fig. 2(a) are difficult to  
 339 distinguish. Both deterministic and stochastic simulations produce realistic-looking ONI  
 340 anomalies sequences. More impressively, the stochastic simulations reproduce huge regional  
 341 emergent patterns including El Niño and La Niña events. In Fig. 2(b), we see canonical El Niño  
 342 anomaly patterns corresponding to El Niño peaks marked in Fig. 2(a) (see also Fig. S11 for map  
 343 sequences). While the deterministic models explain these events as an expression of the  
 344 dynamics implicit in the governing equations, in the stochastic model they emerge from random  
 345 synchronizations from places sharing high  $H$  values (see Fig. 1(a)) and long ocean weather-  
 346 macroweather transition times.

347 StocSIPS also produces realistic and emergent teleconnections patterns: RGI maps, see  
 348 Fig. 2(c) and (d) for lags  $\lambda = 0, 1$  and 3. Despite these striking spatial patterns, there is no  
 349 Granger causality connecting any two points: the optimal predictor is obtained from the past of  
 350 each individual series without any contribution from the teleconnection patterns. These  
 351 correlations do not imply any Granger causality.

## 352 4 Conclusions

353 GCMs long range forecasting skill is low, and this has stimulated the development of  
 354 stochastic alternatives often inspired by correlations. Two competing approaches have  
 355 developed, one that primarily exploits teleconnections (space) with only a short memory in time  
 356 (Markovian), the other – StocSIPS – that only exploits the long memory in time without using  
 357 any spatial information. While Markovian models are approximately initial value problems  
 358 GCMs are strictly so. In comparison, StocSIPS exploits the system’s (scaling) long range  
 359 memory; it is a “past value” model. Although it is tempting to try to improve StocSIPS skill by  
 360 using spatially correlated co-predictors, to be useful the correlations must also be causal.

361 Untangling correlations and causality is possible thanks to the precise notion of Granger  
 362 causality. To apply this, we first extended StocSIPS to the full space-time process, m-StocSIPS,  
 363 that has identical single pixel statistics but that includes pixel-pixel cross-correlations. Although  
 364 m-StocSIPS’s time-lagged temperature cross-correlations are strong, they are generated by  
 365 temporally uncorrelated innovations and it has no Granger causality. For a given position, past  
 366 information from other locations cannot be used to improve on the forecast obtained as an

367 optimal linear combination of past data: those correlations “were already used”. Whereas the  
 368 ultimate causation in deterministic models is their initial conditions, the ultimate cause in  
 369 StocSIPS is its white noise innovations.

370 To make this convincing, we provided a full space-time macroweather model, producing  
 371 global space-time stochastic simulations at one month and 2.5° resolution over 864 months  
 372 (Movie S1). Emergent model properties include realistic teleconnection networks and El Niño  
 373 and La Niña events that have both realistic spatial warming patterns as well as Oceanic El Niño  
 374 indices. For real data, only a finite length of the past series is known, but even in this case, we  
 375 showed that by exploiting the correlations in the temperature series, maximum improvements in  
 376 skill of only 1-2% are possible (and this is in the noise).

377 What then is the status of causal mechanisms such as those linking El Niño events to a  
 378 wet central Asia (Barnston, 2014)? GCMs and StocSIPS provide ultimate causes that eschew  
 379 such mechanisms. At best, it may be argued that ultimate causes initiate a causal chain in which  
 380 an El Niño could be regarded as a proximate cause, and this proximate cause could presumably  
 381 be captured in short memory empirical models. However, thanks to Granger causality we can  
 382 now affirm that at best, at a given pixel  $i$ , the short memory models (partially) compensate for  
 383 their under-exploitation of the memory by effectively “borrowing” the memory of particularly  
 384 strong memory pixels  $j$  such as those in the El Niño region. StocSIPS obviates the need to  
 385 borrow memory from pixel  $j$  by fully exploiting the memory at pixel  $i$ .

### 386 **Acknowledgments**

387 The authors thank Hydro-Québec for a bourse de doctorat Hydro- Québec en science  
 388 (F213013R02). There are no conflicts of interest. We also thank R. Procyk, R. Hébert, and D.  
 389 Clarke for useful discussions. NCEP Reanalysis data provided by the NOAA/OAR/ESRL PSL,  
 390 Boulder, Colorado, USA, from their Web site at <https://psl.noaa.gov/>.

### 391 **References**

- 392 Ali, M. M. (1989). Tests for Autocorrelation and Randomness in Multiple Time Series. *Journal*  
 393 *of the American Statistical Association*, 84(406), 533. <https://doi.org/10.2307/2289939>
- 394 Andree, B. P. J. (2019). Probability, Causality and Stochastic Formulations of Economic Theory.  
 395 *SSRN Electronic Journal*. <https://doi.org/10.2139/ssrn.3422430>
- 396 Barnston, A. (2014). How ENSO leads to a cascade of global impacts. Retrieved November 12,  
 397 2020, from [https://www.climate.gov/news-features/blogs/enso/how-enso-leads-cascade-](https://www.climate.gov/news-features/blogs/enso/how-enso-leads-cascade-global-impacts)  
 398 [global-impacts](https://www.climate.gov/news-features/blogs/enso/how-enso-leads-cascade-global-impacts)
- 399 Biagini, F., Hu, Y., Øksendal, B., & Zhang, T. (2008). *Stochastic Calculus for Fractional*  
 400 *Brownian Motion and Applications*. London: Springer London. [https://doi.org/10.1007/978-](https://doi.org/10.1007/978-1-84628-797-8)  
 401 [1-84628-797-8](https://doi.org/10.1007/978-1-84628-797-8)
- 402 Blender, R., & Fraedrich, K. (2003). Long time memory in global warming simulations.  
 403 *Geophysical Research Letters*, 30(14). <https://doi.org/10.1029/2003GL017666>
- 404 Box, G. E. P., Jenkins, G. M., & Reinsel, G. C. (2008). *Time Series Analysis*. Wiley.  
 405 <https://doi.org/10.1002/9781118619193>
- 406 Brockwell, P. J., & Davis, R. A. (1991). *Time Series: Theory and Methods*. New York, NY:

- 407 Springer New York. <https://doi.org/10.1007/978-1-4419-0320-4>
- 408 Brown, P. T., & Caldeira, K. (2020). Empirical Prediction of Short-Term Annual Global  
409 Temperature Variability. *Earth and Space Science*, 7(6).  
410 <https://doi.org/10.1029/2020EA001116>
- 411 Buchanan, M. (2012). Cause and correlation. *Nature Physics*, 8(12), 852–852.  
412 <https://doi.org/10.1038/nphys2497>
- 413 Bunde, A., Eichner, J. F., Kantelhardt, J. W., & Havlin, S. (2005). Long-Term Memory: A  
414 Natural Mechanism for the Clustering of Extreme Events and Anomalous Residual Times in  
415 Climate Records. *Physical Review Letters*, 94(4), 048701.  
416 <https://doi.org/10.1103/PhysRevLett.94.048701>
- 417 Bunge, M. (2017). *Causality and Modern Science* (4th ed.). Routledge. Retrieved from  
418 <https://books.google.ca/books?id=xCIxDwAAQBAJ>
- 419 CCCma. (2020). The second generation Canadian earth system model (CanESM2). Retrieved  
420 October 29, 2020, from [https://climate-](https://climate-modelling.canada.ca/climatemodeldata/cgcm4/CanESM2/index.shtml)  
421 [modelling.canada.ca/climatemodeldata/cgcm4/CanESM2/index.shtml](https://climate-modelling.canada.ca/climatemodeldata/cgcm4/CanESM2/index.shtml)
- 422 Coeurjolly, J., Amblard, P., & Achard, S. (2010). On multivariate fractional brownian motion  
423 and multivariate fractional Gaussian noise. In *2010 18th European Signal Processing*  
424 *Conference* (pp. 1567–1571).
- 425 Delignières, D. (2015). Correlation Properties of (Discrete) Fractional Gaussian Noise and  
426 Fractional Brownian Motion. *Mathematical Problems in Engineering*, 2015, 1–7.  
427 <https://doi.org/10.1155/2015/485623>
- 428 Donges, J. F., Zou, Y., Marwan, N., & Kurths, J. (2009a). Complex networks in climate  
429 dynamics. *The European Physical Journal Special Topics*, 174(1), 157–179.  
430 <https://doi.org/10.1140/epjst/e2009-01098-2>
- 431 Donges, J. F., Zou, Y., Marwan, N., & Kurths, J. (2009b). The backbone of the climate network.  
432 *EPL (Europhysics Letters)*, 87(4), 48007. <https://doi.org/10.1209/0295-5075/87/48007>
- 433 Eden, J. M., van Oldenborgh, G. J., Hawkins, E., & Suckling, E. B. (2015). A global empirical  
434 system for probabilistic seasonal climate prediction. *Geoscientific Model Development*,  
435 8(12), 3947–3973. <https://doi.org/10.5194/gmd-8-3947-2015>
- 436 Granger, C. W. J. (1969). Investigating Causal Relations by Econometric Models and Cross-  
437 spectral Methods. *Econometrica*, 37(3), 424. <https://doi.org/10.2307/1912791>
- 438 Gripenberg, G., & Norros, I. (1996). On the prediction of fractional Brownian motion. *Journal of*  
439 *Applied Probability*, 33(2), 400–410. <https://doi.org/10.1017/S0021900200099812>
- 440 Hébert, R., & Lovejoy, S. (2018). Regional Climate Sensitivity- and Historical-Based  
441 Projections to 2100. *Geophysical Research Letters*, 45(9), 4248–4254.  
442 <https://doi.org/10.1002/2017GL076649>
- 443 Hirchoren, G. A., & Arantes, D. S. (1998). Predictors for the discrete time fractional Gaussian  
444 processes. In ITS'98 Proceedings. SBT/IEEE International Telecommunications  
445 Symposium (Cat. No.98EX202) (pp. 49–53). IEEE.  
446 <https://doi.org/10.1109/ITS.1998.713090>

- 447 Hosking, J. R. M. (1980). The Multivariate Portmanteau Statistic. *Journal of the American*  
448 *Statistical Association*, 75(371), 602. <https://doi.org/10.2307/2287656>
- 449 Kalnay, E., Kanamitsu, M., Kistler, R., Collins, W., Deaven, D., Gandin, L., et al. (1996). The  
450 NCEP/NCAR 40-Year Reanalysis Project. *Bulletin of the American Meteorological Society*,  
451 77(3), 437–471. [https://doi.org/10.1175/1520-0477\(1996\)077<0437:TNYRP>2.0.CO;2](https://doi.org/10.1175/1520-0477(1996)077<0437:TNYRP>2.0.CO;2)
- 452 Li, W. K., & McLeod, A. I. (1981). Distribution of the Residual Autocorrelations in Multivariate  
453 ARMA Time Series Models. *Journal of the Royal Statistical Society. Series B*  
454 *(Methodological)*, 43(2), 231–239. Retrieved from <http://www.jstor.org/stable/2984853>
- 455 Lovejoy, S. (2018). Spectra, intermittency, and extremes of weather, macroweather and climate.  
456 *Scientific Reports*, 8(1), 12697. <https://doi.org/10.1038/s41598-018-30829-4>
- 457 Lovejoy, S. (2019). Fractional relaxation noises, motions and the fractional energy balance  
458 equation. *Nonlin. Processes Geophys. Discuss., in review.*  
459 <https://doi.org/https://doi.org/10.5194/npg-2019-39>
- 460 Lovejoy, S. (2020). The fractional heat equation. *Geophysical Research Letters*, (in review).
- 461 Lovejoy, S., & de Lima, M. I. P. (2015). The joint space-time statistics of macroweather  
462 precipitation, space-time statistical factorization and macroweather models. *Chaos*, 25(7),  
463 075410. <https://doi.org/10.1063/1.4927223>
- 464 Lovejoy, S., & Schertzer, D. (2013). *The Weather and Climate: Emergent Laws and Multifractal*  
465 *Cascades. The Weather and Climate: Emergent Laws and Multifractal Cascades.*  
466 Cambridge: Cambridge University Press. <https://doi.org/10.1017/CBO9781139093811>
- 467 Lovejoy, S., Del Rio Amador, L., & Hébert, R. (2015). The ScaLIing Macroweather Model  
468 (SLIMM): Using scaling to forecast global-scale macroweather from months to decades.  
469 *Earth System Dynamics*, 6(2), 637–658. <https://doi.org/10.5194/esd-6-637-2015>
- 470 Lovejoy, S., Del Rio Amador, L., & Hébert, R. (2018). Harnessing Butterflies: Theory and  
471 Practice of the Stochastic Seasonal to Interannual Prediction System (StocSIPS). In  
472 *Advances in Nonlinear Geosciences* (pp. 305–355). Cham: Springer International  
473 Publishing. [https://doi.org/10.1007/978-3-319-58895-7\\_17](https://doi.org/10.1007/978-3-319-58895-7_17)
- 474 Lovejoy, S., Procyk, R., Hébert, R., & Del Rio Amador, L. (2020). The Fractional Energy  
475 Balance Equation. *Quarterly Journal of the Royal Meteorological Society*, (in review).
- 476 Ludescher, J., Gozolchiani, A., Bogachev, M. I., Bunde, A., Havlin, S., & Schellnhuber, H. J.  
477 (2014). Very early warning of next El Niño. *Proceedings of the National Academy of*  
478 *Sciences*, 201323058. <https://doi.org/10.1073/pnas.1323058111>
- 479 Lyon, B., & Barnston, A. G. (2005). ENSO and the Spatial Extent of Interannual Precipitation  
480 Extremes in Tropical Land Areas. *Journal of Climate*, 18(23), 5095–5109.  
481 <https://doi.org/10.1175/JCLI3598.1>
- 482 Mandelbrot, B. B., & Van Ness, J. W. (1968). Fractional Brownian Motions, Fractional Noises  
483 and Applications. *SIAM Review*, 10(4), 422–437. <https://doi.org/10.1137/1010093>
- 484 NCEP/NCAR. (2020). NCEP/NCAR Reanalysis 1. Retrieved January 3, 2020, from  
485 <https://www.esrl.noaa.gov/psd/>
- 486 Palma, W. (2007). *Long-Memory Time Series*. Hoboken, NJ, USA: John Wiley & Sons, Inc.



- 487 Palmer, T. N. (2019). Stochastic weather and climate models. *Nature Reviews Physics*, *1*(7),  
488 463–471. <https://doi.org/10.1038/s42254-019-0062-2>
- 489 Poskitt, D. S., & Tremayne, A. R. (1982). Diagnostic Tests for Multiple Time Series Models.  
490 *The Annals of Statistics*, *10*(1), 114–120. Retrieved from  
491 <http://www.jstor.org/stable/2240503>
- 492 Del Rio Amador, L., & Lovejoy, S. (2019). Predicting the global temperature with the Stochastic  
493 Seasonal to Interannual Prediction System (StocSIPS). *Climate Dynamics*, *53*(7–8), 4373–  
494 4411. <https://doi.org/10.1007/s00382-019-04791-4>
- 495 Del Rio Amador, L., & Lovejoy, S. (2020). Using regional scaling for temperature forecasts with  
496 the Stochastic Seasonal to Interannual Prediction System (StocSIPS). *Climate Dynamics*,  
497 (submitted).
- 498 Rypdal, K., Østvand, L., & Rypdal, M. (2013). Long-range memory in Earth’s surface  
499 temperature on time scales from months to centuries. *Journal of Geophysical Research:*  
500 *Atmospheres*, *118*(13), 7046–7062. <https://doi.org/10.1002/jgrd.50399>
- 501 Steinhäuser, K., Ganguly, A. R., & Chawla, N. V. (2012). Multivariate and multiscale  
502 dependence in the global climate system revealed through complex networks. *Climate*  
503 *Dynamics*, *39*(3–4), 889–895. <https://doi.org/10.1007/s00382-011-1135-9>
- 504 Straškraba, M. (2007). K. W. Hipel and A. I. McLeod: Time Series Modelling of Water  
505 Resources and Environmental System. 1013 pp. Amsterdam, Elsevier, 1994, XXXII. ISBN  
506 0–444–89270–2. Available from Elsevier Science Publishers B. V., Order Fulfilment  
507 Department. P.O. Box 211, 10. *Internationale Revue Der Gesamten Hydrobiologie Und*  
508 *Hydrographie*, *80*(1), 60–60. <https://doi.org/10.1002/iroh.19950800107>
- 509 Sugihara, G., May, R., Ye, H., Hsieh, C. -h., Deyle, E., Fogarty, M., & Munch, S. (2012).  
510 Detecting Causality in Complex Ecosystems. *Science*, *338*(6106), 496–500.  
511 <https://doi.org/10.1126/science.1227079>
- 512 Tsonis, A. A. (2018). Insights in Climate Dynamics from Climate Networks. In *Advances in*  
513 *Nonlinear Geosciences* (pp. 631–649). Cham: Springer International Publishing.  
514 [https://doi.org/10.1007/978-3-319-58895-7\\_29](https://doi.org/10.1007/978-3-319-58895-7_29)
- 515 Tsonis, A. A., Swanson, K. L., & Roebber, P. J. (2006). What Do Networks Have to Do with  
516 Climate? *Bulletin of the American Meteorological Society*, *87*(5), 585–596.  
517 <https://doi.org/10.1175/BAMS-87-5-585>
- 518 Varotsos, C. A., Efstathiou, M. N., & Cracknell, A. P. (2013). On the scaling effect in global  
519 surface air temperature anomalies. *Atmospheric Chemistry and Physics*, *13*(10), 5243–5253.  
520 <https://doi.org/10.5194/acp-13-5243-2013>
- 521 Wold, H. (1938). A Study in Analysis of Stationary Time Series. *Journal of the Royal Statistical*  
522 *Society*.
- 523 Yamasaki, K., Gozolchiani, A., & Havlin, S. (2008). Climate Networks around the Globe are  
524 Significantly Affected by El Niño. *Physical Review Letters*, *100*(22), 228501.  
525 <https://doi.org/10.1103/PhysRevLett.100.228501>